Atmósfera (1997), **10**, *pp. 23-42*

On intermonthly oscillations in the atmosphere, part II

A. WIIN-NIELSEN

Geophysical Department, University of Copenhagen, Juliane Maries Vej 30, 2100 Copenhagen Ø, Denmark

(Manuscript received May 8, 1996; accepted July 10, 1996)

RESUMEN

El trabajo explora la posibilidad de que las variaciones intermensuales observadas en la atmósfera puedan ser descritas por un modelo no lineal, de bajo orden, conteniendo nueve componentes. El modelo es formulado sobre un plano-f y contiene solamente interacciones de onda con onda. Está basado en la atmósfera barotrópica equivalente formulada de tal manera que contiene tanto calentamiento como disipaciones. Los números de onda varían de 1 a 3 en ambas direcciones zonal y meridional. La mayoría de las integraciones del modelo suponen que las oscilaciones son un fenómento planetario y, por consiguiente, han sido formuladas con una máxima longitud de onda de 28000 km.

Los resultados muestran que los periodos observados (30 a 35, 45 y 70 días) pueden ser reproducidos por el modelo. Otros periodos se encuentran también, pero son principalmente de pequeñas amplitudes. El modelo permite una determinación del patrón de calentamiento necesario para producir las oscilaciones observadas. Se requiere que el nivel de calentamiento esté arriba del calentamiento coronológico promediado en la atmósfera, y el calentamiento es tal que muestra un fuerte gradiente de calentamiento meridional.

La investigación es una continuación de un intento previo de modelar oscilaciones intermensuales, usando un muy simple modelo de tres componentes, basado en la primera ecuación del movimiento con advección no lineal y forzamiento del momento y disipación.

El nuevo modelo permite una descripción más física del fenómeno.

ABSTRACT

The investigation explores the possibility that the observed intermonthly variations in the atmosphere may be described by a nonlinear low-order model containing nine components. The model is formulated on a f-plane and contains only wave-wave interactions. It is based on the equivalent barotropic atmosphere formulated in such a way that it contains both heating and dissipations. The wave numbers vary from 1 to 3 in the zonal and the meridional direction. Most of the integrations of the model assume that the oscillations are a planetary phenomenon, and they have therefore been performed with a maximum wavelength of 28000 km.

The results show that the observed periods (30-35, 45 and 70 days) may be reproduced by the model. Other periods are also found, but they are mainly of small amplitudes. The model permits a determination of the heating pattern necessary to produce the observed oscillations. It is required that the heating level is above the time-averaged heating in the atmosphere, and the heating is such that it displays a strong meridional heating gradient.

The investigation is a continuation of an earlier attempt to model intermonthly oscillations using a very simple three-component model based on the first equation of motion with non-linear advection and momentum forcing and dissipation. The new model permits a more physical description of the phenomena.

1. Introduction

The present paper will deal with the inter-monthly oscillations in the atmosphere. An earlier paper (Wiin-Nielsen, 1996), hereafter referred to as Part I, contains an extended list of references on the subject. References in the present paper will therefore be restricted to those that are directly relevant to the present study.

In Part I it was shown that some aspects of the intermonthly oscillations, determined from observations by Plaut and Vautard (1994), could be simulated by a simple three-component model based on the nonlinear first equation of motion with Newtonian momentum forcing and dissipation. Only one space variation (x) and time (t) was permitted in Part I. While the model could reproduce the observed periods of oscillations, it was so simple that many pertinent questions concerning the oscillations could not be answered.

It was, however, also shown in Part I, that a low-order six-component model formulated on the sphere and including the first three planetary waves could also reproduce essentially the same periods as the simple model with only one space dimension. It should be pointed out that the spherical model contained also a Newtonian forcing and thus no explicit heating.

The purpose of the present investigations is to generalize the model in Part I to include atmospheric heating and cooling as well as dissipation and to permit variations in both the x- and the y-directions. From a formal point of view this can be done in a simple way by using the equivalent barotropic assumption in both the vorticity equation and in the thermodynamic equation as shown in the appendix of Wiin-Nielsen (1991). While this approach will be used in the present model, it is realized that the low-order model so derived does not contain the influences of the atmospheric temperature advection.

2. The model

The model is based on the vorticity equation in the form:

$$\frac{\partial \zeta}{\partial t} + \vec{\nu} \cdot \nabla(\zeta + f) = f_o \frac{\partial \omega}{\partial p} + g \frac{\partial \vec{k} \cdot \nabla \times \vec{\tau}}{\partial p} \tag{2.1}$$

in which ζ is the vertical component of the vorticity, f the Coriolis parameter, ω the vertical p-velocity, p the pressure and the last term gives the vertical change of the curl of the stress.

The second basic equation is the thermodynamic equation in the form:

$$\frac{\partial}{\partial t}[\frac{\partial \Psi}{\partial p}] + \vec{\nu} \cdot \nabla[\frac{\partial \Psi}{\partial p}] + \frac{\sigma}{f_o}\omega = -\frac{R}{c_p f_o p} H \tag{2.2}$$

in which Ψ is the streamfunction, σ is the static stability parameter, R the gas constant, c_p the specific heat for constant pressure, and H the heating per unit mass and unit time.

For each of the quantities: the streamfunction, the vorticity and the two components of the horizontal wind we introduce an equivalent barotropic assumption

$$a = A(p)\overline{a}$$

$$\overline{a} = \frac{1}{p_o}\int_o^{p_o} a\,dp \tag{2.3}$$

in which the bar indicates a vertical average as defined in (2.3).

Using (2.3) it is seen that the advection term in the thermodynamic equation vanishes. Inherently, we assume therefore that the intermonthly oscillations that we want to describe also are of an equivalent barotropic nature. Following the derivation given in Wiin-Nielsen (1991) we get after elimination of the vertical p-velocity the equation:

$$\frac{\partial[\nabla^2\Psi - q^2\psi]}{\partial t} + \vec{\nu}\cdot\nabla(\zeta + f) = -\gamma H_o - \varepsilon\zeta \tag{2.4}$$

We give finally the expressions for the coefficients in eq. (2.4):

$$q^2 = -\frac{f_o^2}{\sigma_o p_o^2}[\frac{dA}{d\pi}]_1$$

$$\pi = \frac{p}{p_o}$$

$$\gamma = \frac{f_o}{\sigma_o p_o^2}\frac{R}{c_p}\overline{A^2} \tag{2.5}$$

ε is a measure of the intensity of the dissipation in the boundary layer. The numerical value is estimated using the normal approximation for the surface stress.

Equation (2.5) is valid at the equivalent barotropic level, where the horizontal divergence vanishes. We may therefore express the horizontal wind in terms of the streamfunction. The vertical velocity may then be calculated at any time that it is wanted from the equivalent barotropic assumptions. Since many integrations have to be made of the basic equation it is of importance to make these as efficient as possible. In the numerical integration of eq. (2.4) it is an advantage to use non-dimensional quantities. The scaling has been done as inticated in eq. (2.6) and the resulting equation is given in (2.7) with $k = 2\pi/L$:

$$\Psi = k^{-2}\varepsilon\hat{\Psi}$$

$$t = \varepsilon^{-1}\hat{t}$$

$$H_o = 10^{-3}\hat{H}_o \tag{2.6}$$

$$\frac{\partial(\hat{\zeta} - s^2\Psi)}{\partial\hat{t}} = J(\hat{\zeta},\hat{\Psi}) - \frac{\beta}{k\varepsilon}\hat{\nu} - \frac{\gamma 10^{-3}}{\varepsilon^3}\hat{H}_o - \hat{\zeta}$$

$$s^2 = \frac{q^2}{k^2} \tag{2.7}$$

Based on eq. (2.7) a low-order model has been created. Numerous possibilities exist for the selection of the components that are included in the model. In this particular case we want to

emphasize wave-wave interactions. A dependent variable such as the stream-function and the heating has therefore been selected in the following way:

$$a(x,y,t) = \sum_{n=1}^{3}\sum_{m=1}^{3} A(m,n,t)\sin(n\mu y)\sin(m\lambda x) \tag{2.8}$$

where a is an arbitrary variable. The particular selection has its limitations. Since only sine-functions are included, we will be dealing with standing oscillations. In addition, the beta-effect and the rôle of the zonal current and its interactions with the waves will be excluded from the model. Both of these limitations can be removed by generalizing the basic specification to the following form:

$$a(x,y,t) = \sum_{n=1}^{3}\sum_{m=1}^{3} \sin(n\mu y)[A(m,n,t)\sin(m\lambda x) + B(m,n,t)\cos(m\lambda x)] \tag{2.9}$$

in which case the waves will move and the beta-effect can be retained. It was, however, decided to stay with the nine equations specified through (2.8) and to use more general models at a later time, depending on the results obtained from the present investigation.

Appendix I contains the nine equations in detail, while Appendix II gives the formulas for all the coefficients that are constants in each particular integration of the set of ordinary, coupled, nonlinear equations. The integrations have in each case been carried out by using the lowest order Runge-Kutta scheme, the so-called Heun scheme. The equations have been integrated for several years to ensure that the initial state has no influence on the final result. The curves to be shown later cover a suitable interval of time at the end of the integrations.

We have also assumed from the very beginning that the observed oscillations are of a planetary nature and are due to nonlinear interactions among the three longest waves. The smallest wave number corresponds thus to a wavelength of 28000 km which is approximately the circumference of the Earth at 45 degrees of latitude.

3. Results from the 9-component model

The first condition which has to be satisfied in order to obtain a limit cycle is a sufficiently large gradient in the imposed heating. The period of the limit cycle is determined by a frequency analysis of one of the dependent variables for a suitable time period at the end of the long integration.

To illustrate the behavior of the model with respect to the period of response we show some examples. Figure 1 shows the amplitude of the response as a function of h1 in a case where h2=55.0 and h3=25.0, while all the remaining values of the heating components are zero. (The symbols hn used here and in the figures are the same as the notation h_n in the formulas). For negative values of h1<-0.5 we find a period of 70 days. The amplitude is zero for h1=-30.0 (stability) and has a maximum for h1=-25.0. Smaller amplitudes are found for -25.0<h1<-0.5, and at h1=-0.5 the model is again stable. Figures 2 and 3 show the heating distribution in the two cases resulting in a stable stationary state (h1=-18 and h1=-0.5). For h1>-0.5 we obtain again a series of limit cycles with a period of 52.5 days, but it is seen that the amplitudes are smaller than those obtained for negative values of h1.

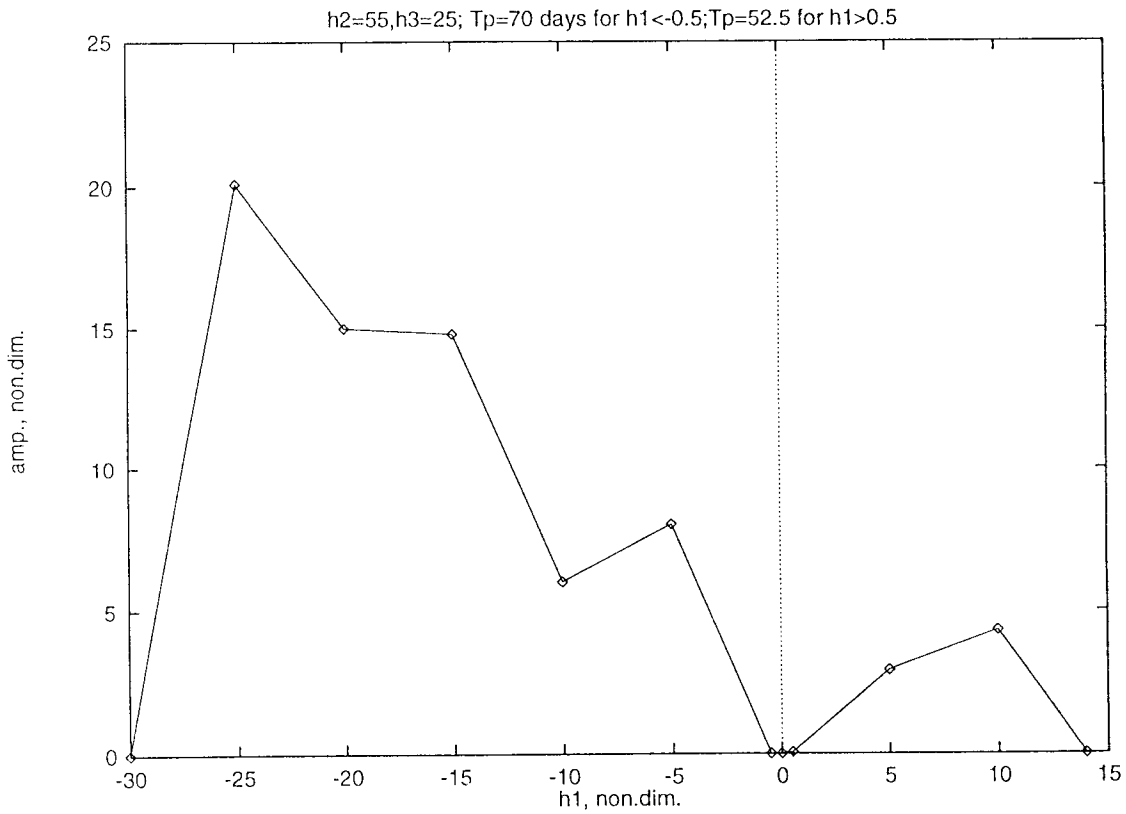

Fig. 1. The amplitude of a 70 day oscillation as a function of the heating parameter h1 keeping h2=55 and h3=25. Other heating components are zero.

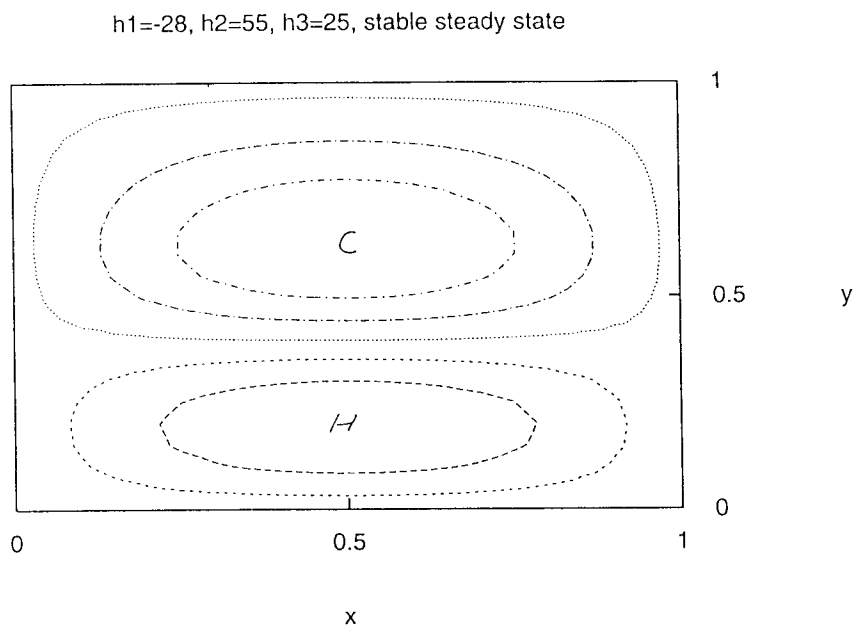

Fig. 2. The distribution of the heating for h1=-28, h2=55 and h3=25. Other heating components are zero. This configuration results in a stable steady state.

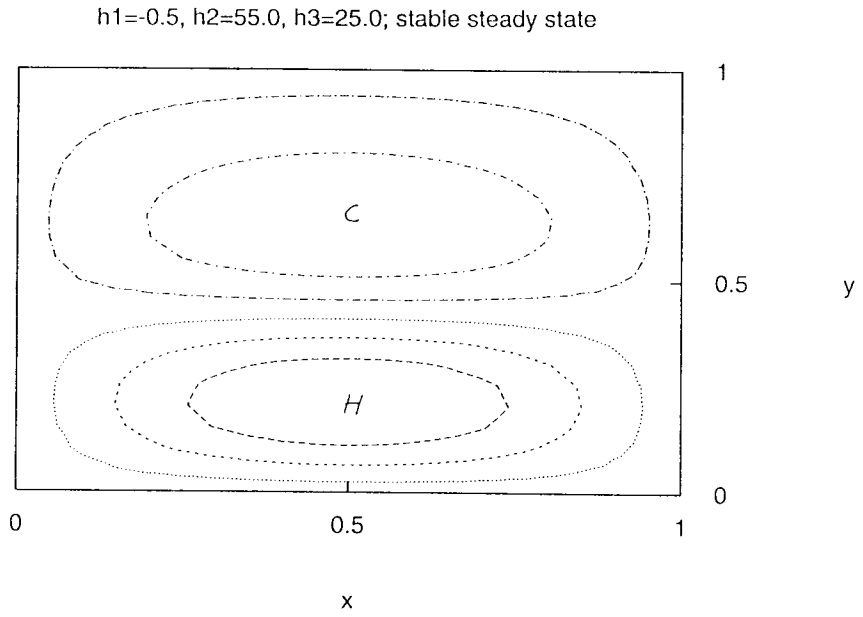

Fig. 3. The distribution of the heating for h1=-0.5, h2=55 and h3=25. Other heating components are zero. This configuration results in a stable steady state.

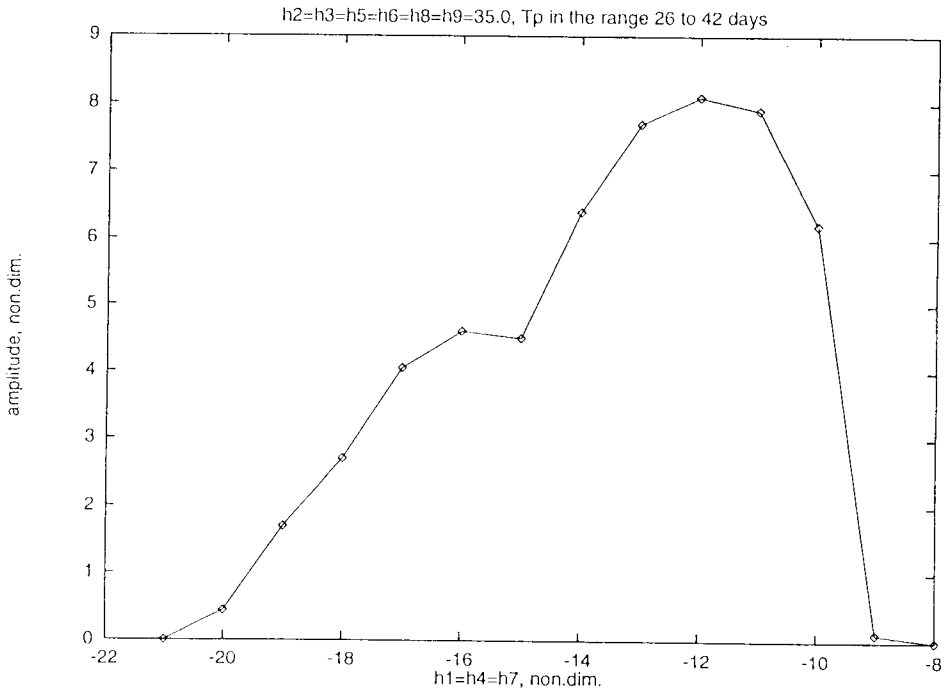

Fig. 4. The amplitude of an oscillation as a function of h1 = h4 = h7. h2= h3= h5= h6= h8= h9= 35. Periods range from 26 to 42 days.

Similar behavior may be obtained for other values of the heating parameters. Figure 4 gives an example. In this series of experiments we have always kept h1=h4=h7=H and the remaining heating parameters are set at 35.0. It is then seen that limit cycles are obtained for $-21 < H < -8$, while stable steady states are found for H=-21 and -8. The periods are 30 to 35 days for $-20 < H \leq$-16 and 40 to 45 days for -15$\leq$H$\leq$-9. Figure 5 shows the typical heating pattern for the left part of Figure 4 dominated by periods of about 30 to 35 days. It is seen that these periods may appear when the heating distribution is more localized than in Figures 2 and 3, and

where the cooling to the north is more intense than the heating to the south. Figure 6 shows the heating distribution for the right part of Figure 4 dominated by periods of 40 to 45 days. These oscillations may then appear also for a localized heating, but in the case of Figure 6 heating is more intense to the south than the cooling is to the north.

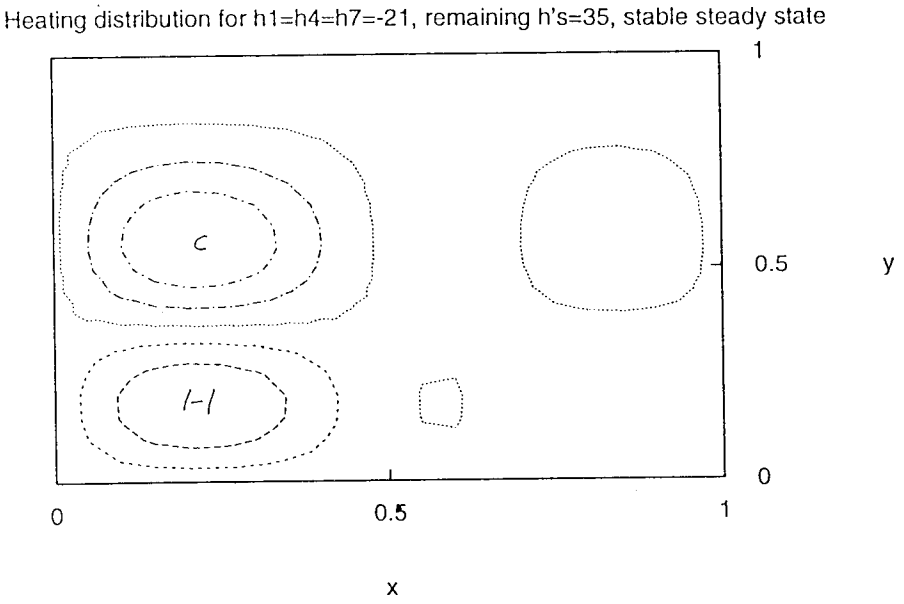

Fig. 5. Heating distribution for h1=h4=h7=-21, other heating components are equal to 35.

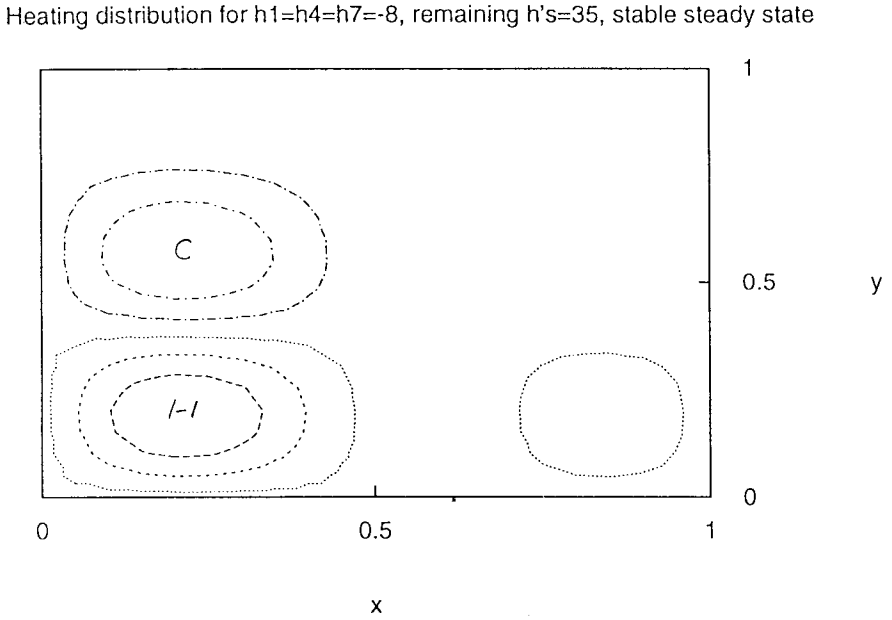

Fig. 6. Heating distribution for h1=h4=h7=-8, other heating components are equal to 35.

As in Part I it has not been attempted to cover the 9-dimensional space of the amplitudes of the heating function and to record the model response in each case. Three examples of oscillations, each corresponding for a specific period, will be presented.

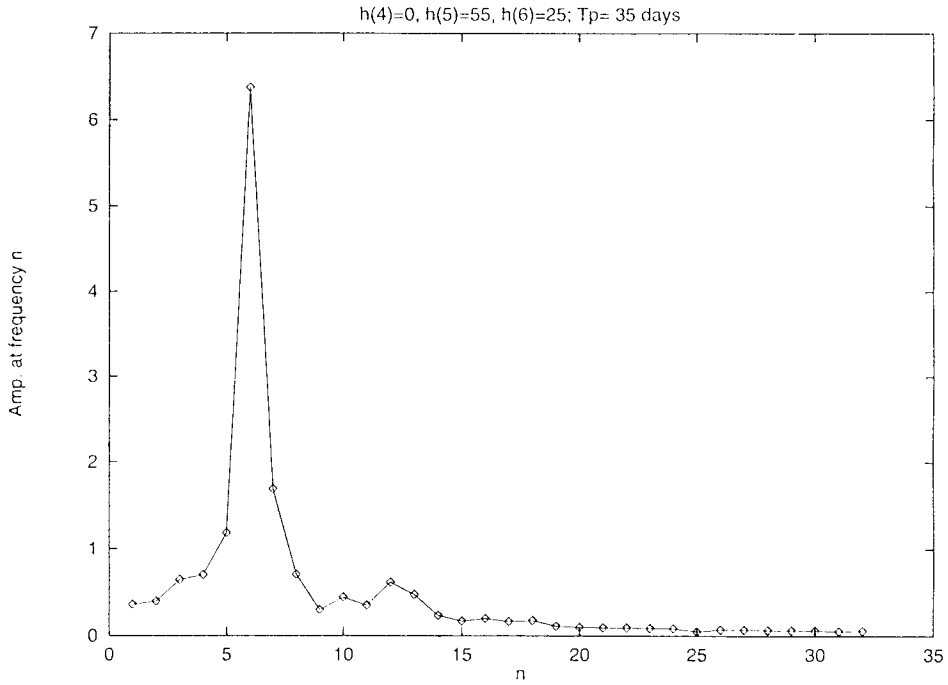

Fig. 7a. Frequency diagram for a case with h5=55 and h6=25. The period is 35 days.

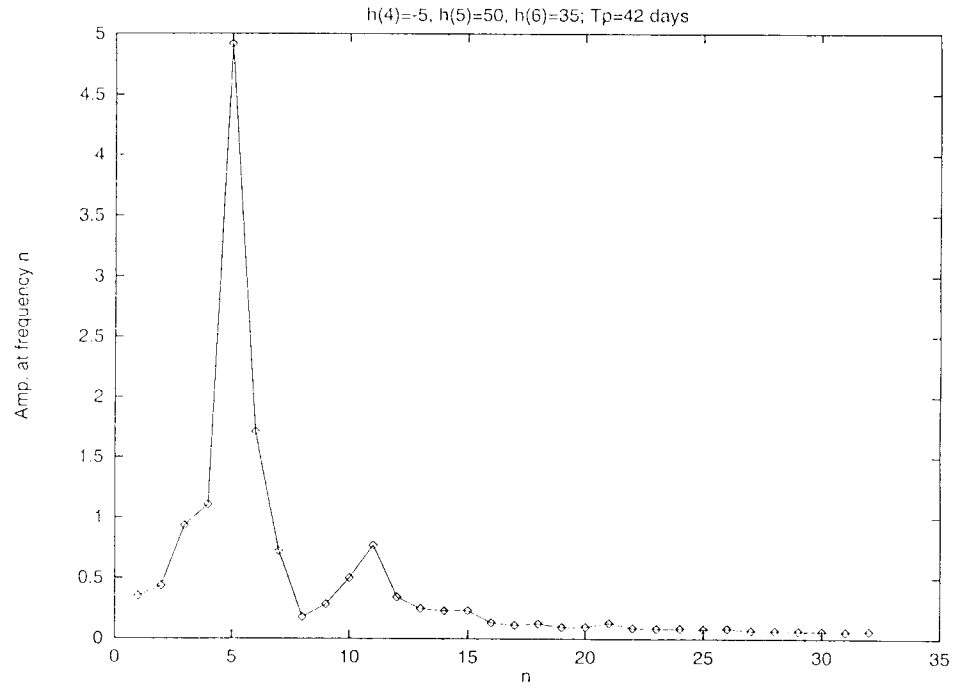

Fig. 7b. Frequency diagram for the case of h4=-5, h5=50 and h6=35. The period is 42 days.

Figure 7a shows the frequency analysis for a case with h5=55 and h6=35, while all the other heating components were set to zero. The frequency analysis was performed using a total of 210 days. It is thus seen that the period in this case is 35 days. Figure 7b is the corresponding diagram for the case of h4=-5, h5=50 and h6= 35 with all other heating components set to zero. The maximum response is at n=5 corresponding to 42 days. Figure 7c is for the case h5=40 with the remaining components set to zero. The maximum response is in this case at n=3 corresponding to 70 days. The limit cycles are simple in some cases and complicated in others. Figures 8a to 8c show, for a case with h4=-1, h5=60 and h6=+1, the projections of the limit cycle on the three planes as indicated in the figures. All the curves show clearly the periodicity of the oscillations since none of them indicate a beginning or an end. It is, however also obvious that oscillations with smaller periods are present in the limit cycle. This can also be seen from Figure 9 containing the frequency analysis for the same case.

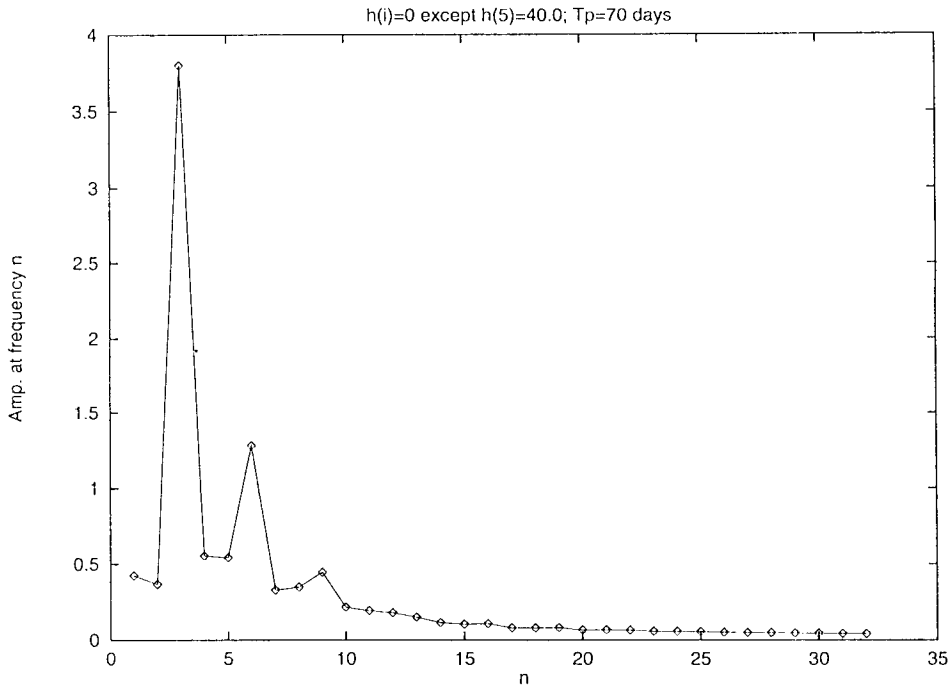

Fig. 7c. Frequency diagram for h5=40. Other heating components are zero. The period is 70 days.

Illustrations similar to Figures 8a, 8b and 8c could naturally be prepared for the x- and the z-variables. However, it may be more instructive to look at the field of the stream-function at times separated by half a period. For this purpose Figure 10a and Figure 10b have been prepared. They refer to the same case as Figures 8 and 9. As explained in Section 2 the present model does not contain neither a zonal current nor a beta-effect. The model is therefore capable of producing standing oscillations only as seen in Figure 10a and 10b where the oscillation is between a low and a high in the center of the channel.

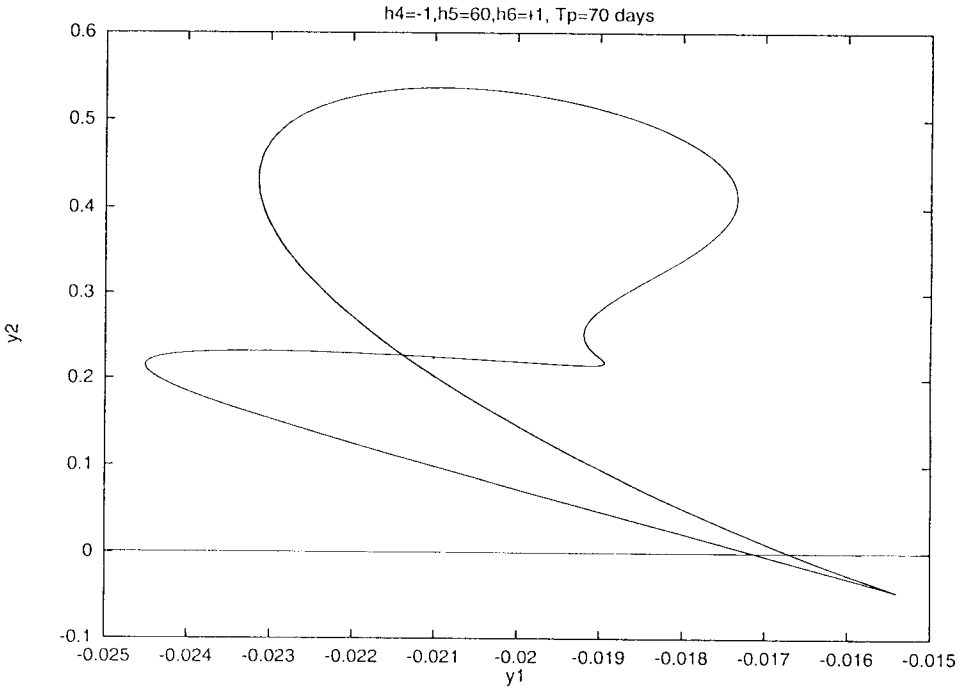

Fig. 8a. Projection of a limit cycle on the y1, y2 plane. h4=-1, h5=60 and h6=1.

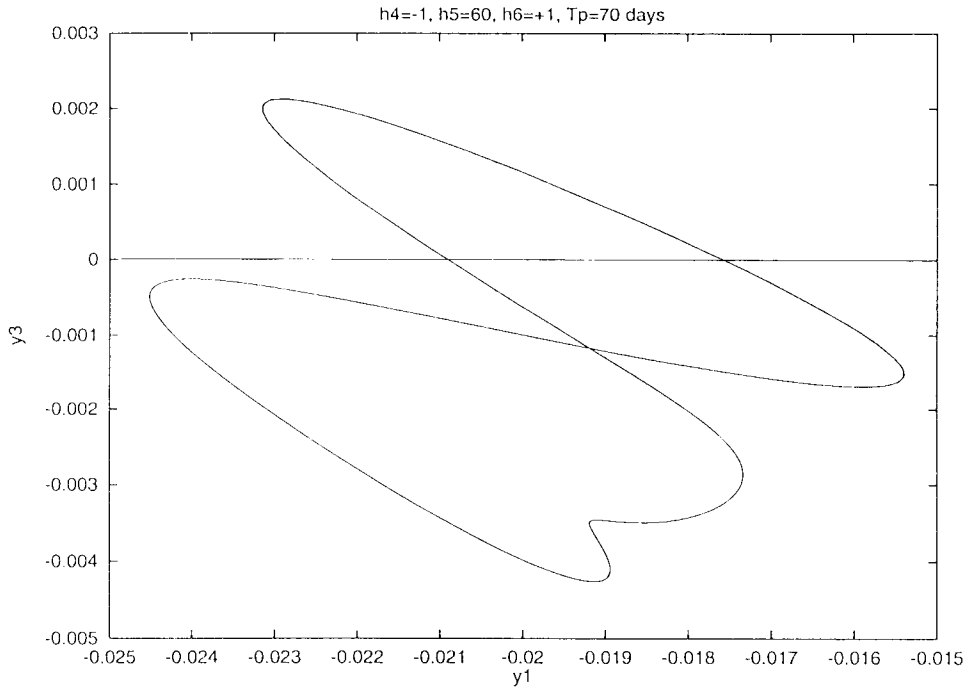

Fig. 8b. Projection of the same limit cycle as in Fig. 8a on the y1, y3 plane.

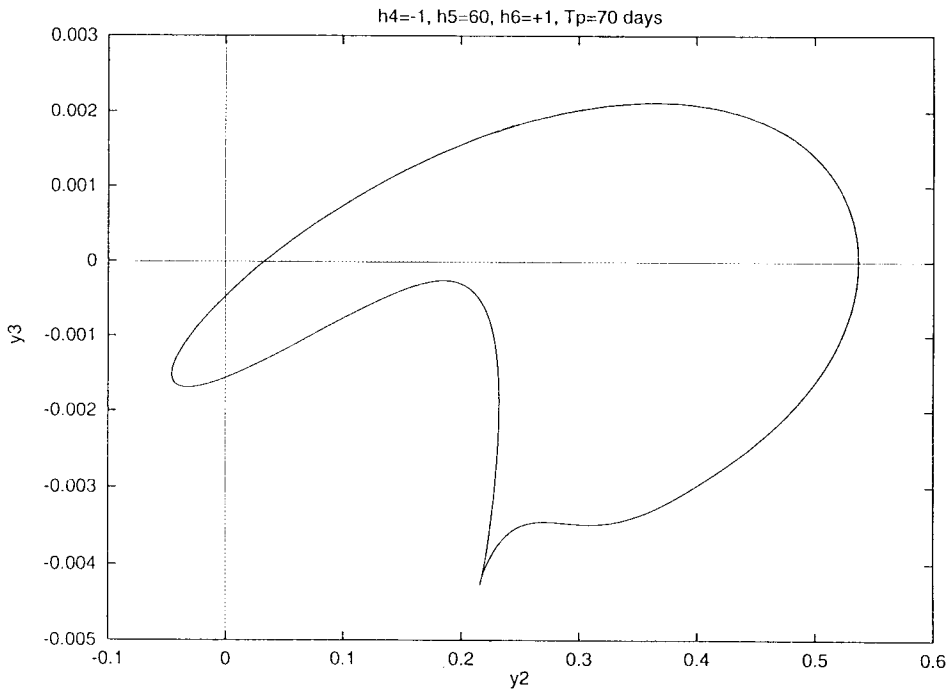

Fig. 8c. Projection of the same limit cycle as in Fig. 8a on the y2, y3 plane.

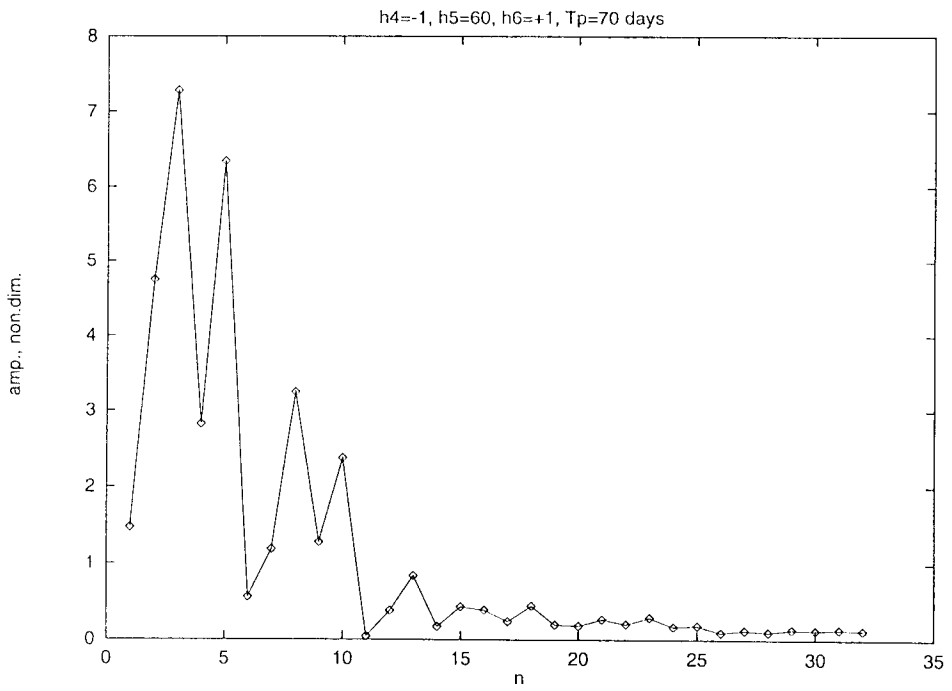

Fig. 9. Frequency diagram for the case displayed in Figs. 8a, 8b and 8c.

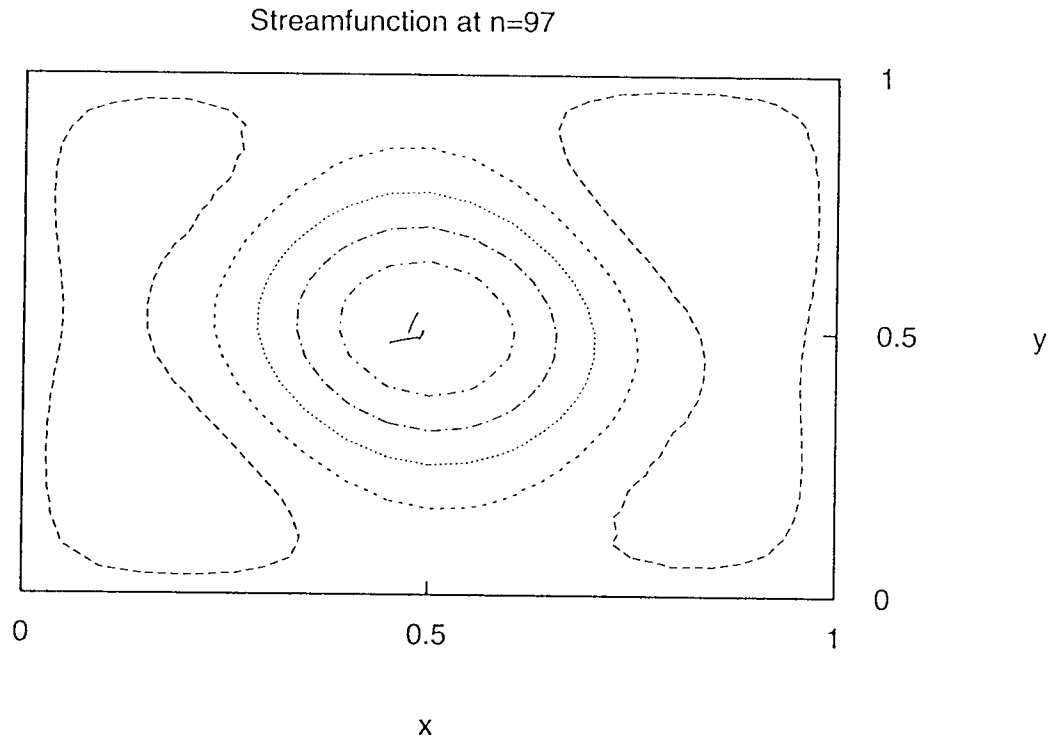

Fig. 10a. The streamfunction at n=97 for the experiment in Figs. 8a, 8b and 8c

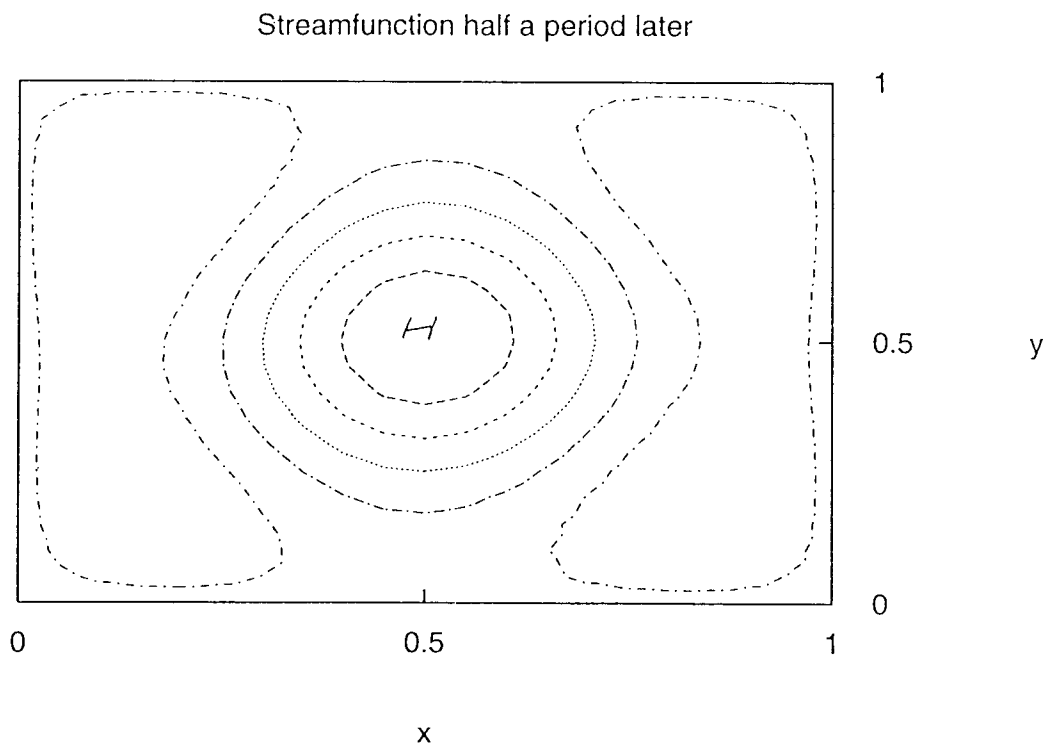

Fig. 10b. The streamfunction half a period later than the time for Fig. 10a.

4. A model with the beta-effect

The main purpose of the present section is to show that the intermonthly oscillation appear also in low-order models with the beta-effect which was excluded in the nine-component model.

From the paper by Wiin Christensen and Wiin-Nielsen (1996) we know that limit cycles may appear in a spherical model with six components. However, only a couple of cases were investigated leading to a 35 day oscillation. Using the same model we shall in the present section expand the search for limit cycles with other periods. In the examples shown below we have in all cases limited the forcing to the x-components of the six component model. Thus, the components y1f, y2f and y3f are zero in all cases. We shall illustrate the model behavior by a number of examples.

The first example will show a 70 day oscillation. As in the previous section it is found that low values of the heating components result in stable steady states. Increasing the intensity of the heating oscillations start to appear. After a number of experiments it was found that relatively large values of the heating on components 2 and 3 combined with a small cooling on component 1 resulted in 70 day oscillations. Figure 11 gives an example with $x_{1f} = -1.0 \times 10^{-3}$, $x_{2f} = 2.2 \times 10^{-2}$ and $x_{3f} = 2.5 \times 10^{-2}$. The main response corresponds to a period of 70 days, since sampling is done over a period corresponding to 630 days, but smaller amplitude are also found on the sub-harmonics n=18 and n=27.

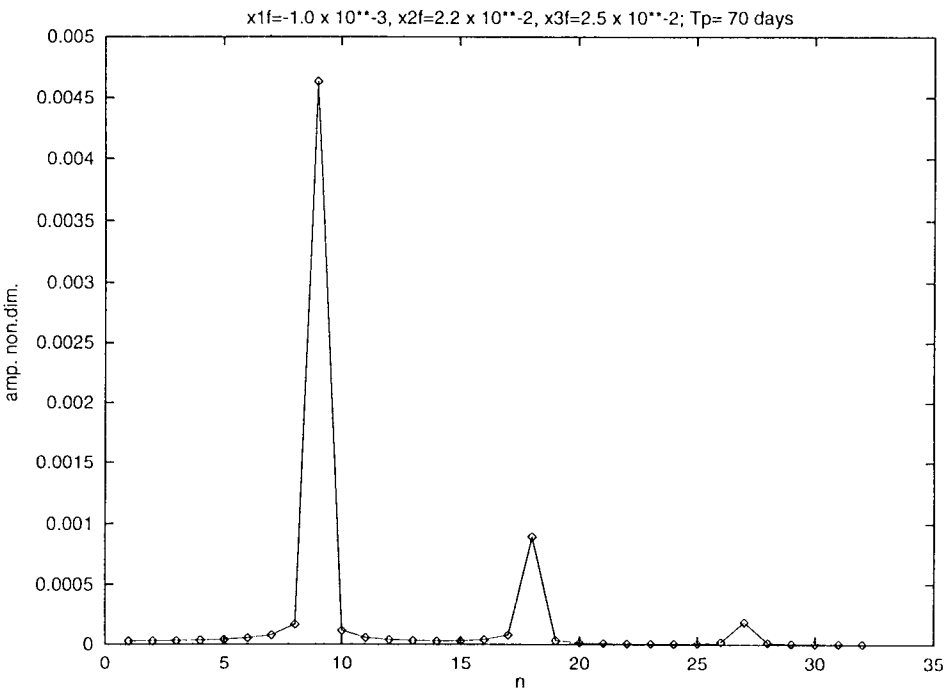

Fig. 11. Frequency diagram for $x_{1f} = -1.0 \times 10^{-3}$, $x_{2f} = 2.2 \times 10^{-2}$ and $x_{3f} = 2.5 \times 10^{-2}$. The period is 70 days.

Additional experimentation resulted in a combination of heating components giving a period of 45 days. The frequency diagram in Figure 12 was obtained for $x_{1f} = 2.3 \times 10^{-2}$, $x_{2f} = 4.3 \times 10^{-2}$ and $x_{3f} = 3.6 \times 10^{-2}$. When x_{3f} is increased the experiments show the same period of 45 days, but a change is observed when x_{3f} reaches a value of about 3.7×10^{-2}. For the value 3.731×10^{-2} one still observes a main response at a period of 45 days, but for $x_{3f} = 3.732 \times 10^{-2}$ a major change is beginning to take place. In addition to the maximum at n=14 (45 days) one observes secondary maxima at n=10 (63 days) and at n= 20 (34.5 days) as shown in Figure 13. A further slight increase to the value $x_{3f} = 3.733 \times 10^{-2}$ results in a frequency diagram given in Figure 14 where the major response in at n=21 (30 days) and a secondary maximum for n=10 (63 days). Thereafter the period of 30 days is found when x_{3f} is increased up to a value of 4.187×10^{-2}.

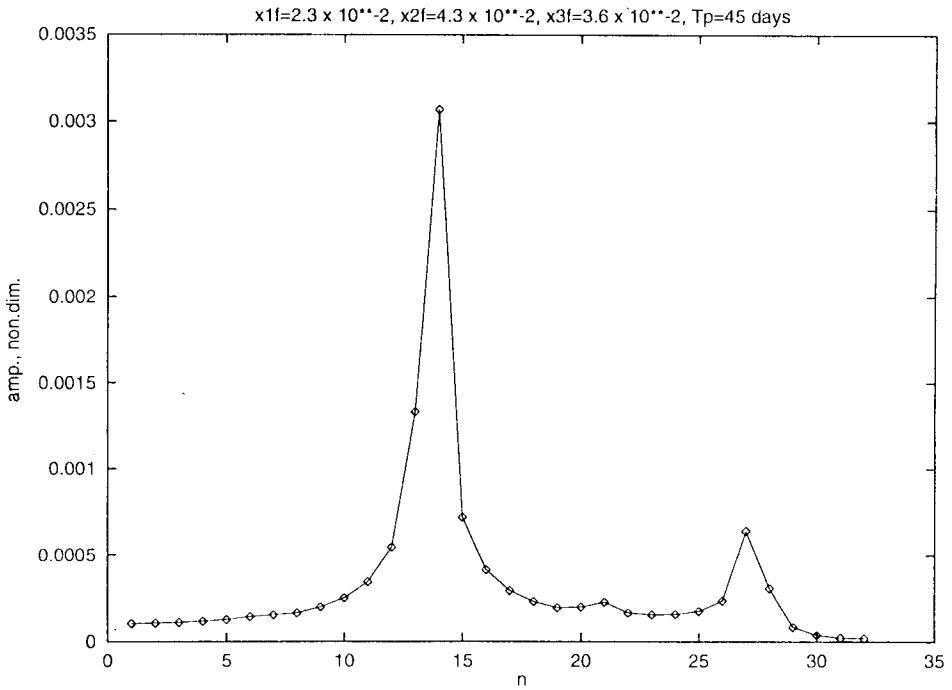

Fig. 12. Frequency diagram for $x_{1f} = 2.3 \times 10^{-2}$, $x_{2f} = 4.3 \times 10^{-2}$ and $x_{3f} = 3.6 \times 10^{-2}$. The period is 45 days.

However, for $x_{3f} = 4.188 \times 10^{-2}$ the frequency diagram changes suddenly to show a periodic oscillation of 45 days as seen in Figure 15.

It has thus been shown that the major observed periods of 30, 35, 45 and 70 days can be found using the spherical 6-component model.

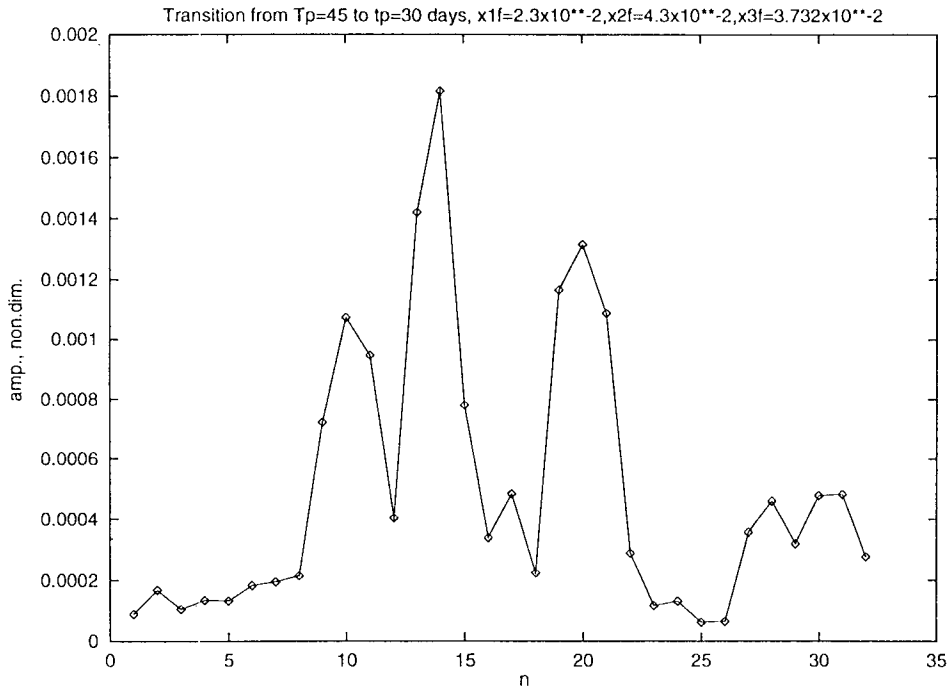

Fig. 13. Frequency diagram $x_{3f} = 3.732 \times 10^{-2}$ while the other values are as in Figure 12. Note that the major response is still n=14, but secondary maxima appear at n=10 and n=20.

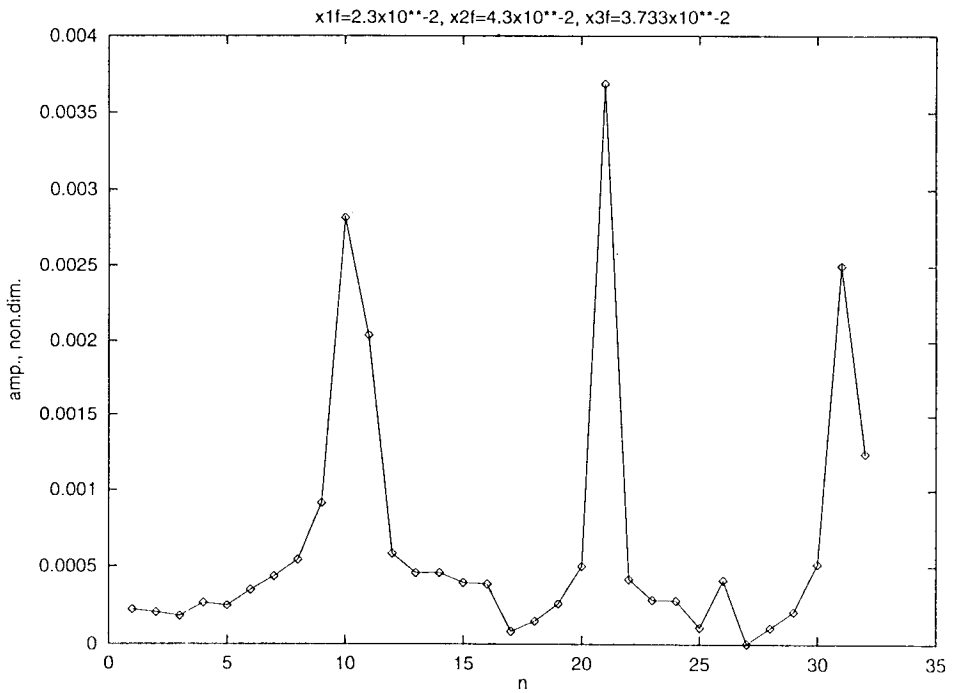

Fig. 14. Frequency diagram for $x_{3f} = 3.733 \times 10^{-2}$ while other values are as in Figure 12. The main response is now at n=21 (30 day period).

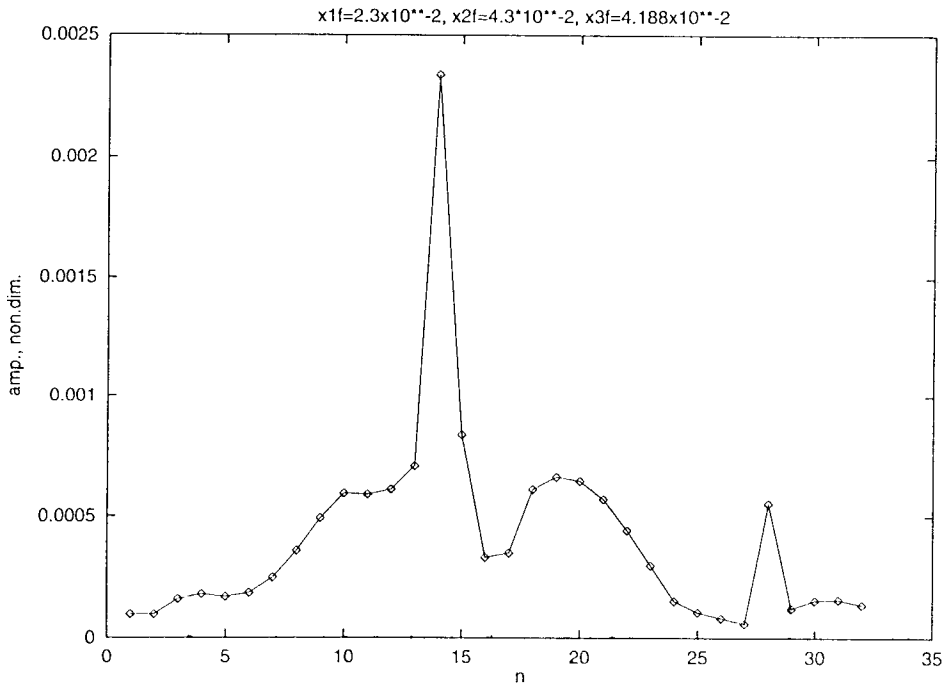

Fig. 15. Frequency diagram for $x_{3f} = 4.188 \times 10^{-2}$ while other values are as in Figure 12. It is seen that the period is once again 45 days.

5. Concluding remarks and suggestions for further work

The investigation presented in this paper is more realistic than the one in Part I. Although the integrations are based on a simple low-order model it is possible to incorporate atmospheric heating and dissipation. The results show that the heating has to have a south-north gradient that is sufficiently large to create limit cycles. If such a condition is not fulfilled the model will converge towards a stable steady state.

By varying a single component of the heating while keeping the other components constant it has been demonstrated that limit cycles typically appear within a certain range of the changing heating component. Stable steady states are found at both ends of the interval. Within the range limit cycles occur. The amplitudes and the periods of the limit cycles are small adjacent to the endpoints while a larger amplitude of the limit cycle is found in the central part of the interval. It is also found for large values of the changing heating component that the amplitude and the period may continue to increase, but this behavior is observed for unrealistically large values of the forcing.

As illustrated by examples the shorter periods of the intermonthly oscillations (30-35 days) will appear when the heating gradient is localized as seen in Figures 5 and 6, while the longer period oscillations (about 70 days) will appear when the heating gradient is of a global nature as seen in Figure 2. The localized heating pattern are obtained by superposition of the three long waves incorporated in the model. However, it is possible that the various oscillations may occur during other heating patterns since it has not been possible to cover all combinations in the six dimensional space of possible heating components.

The main conclusion reached in Part I may therefore be maintained for the present more physically based model. The observed intermonthly oscillations seem to be a result of larger than normal heating intensity on regional or global scales. A localized heating will produce the smaller periods and the global heating patterns will produce the longer periods of the limit cycles. As stated in Part I it will be interesting to investigate whether or not these conclusions obtained from a model with very few degrees of freedom are true also for a general circulation model with a large number of degrees of freedom. Experiments of this kind could be done by specifying the heating patterns in advance and to keep them constant during the integration of the model, but a better experiment would be to incorporate a physical mechanism that gradually would increase the heating to a level where the intermonthly oscillations would be created by the model. Supposedly, it would then be possible also to investigate the conditions under which the intermonthly oscillations would disappear in the model.

The model described in the present paper suffers from the neglect of the beta-effect. It is thus also necessary to investigate a low-order model including the variation of the Coriolis parameter. In the present paper we have looked at the problem by adopting an earlier model which is formulated on the spherical Earth and contain six components We know already from the results of Wiin Christensen and Wiin-Nielsen (1996) that limit cycles appear also when the full variation of the Coriolis parameter is included in low order models, but a more extensive investigation has been made in this paper. In addition, the whole question of intermonthly oscillations should be explored by applying baroclinic models. It is hoped that a return to these questions will be possible in the future.

APPENDIX I

The equations describing the model are based on the following expression for the streamfunction:

$$\Psi(x,y,t) = \sin(kx)[x_1\sin(\mu y) + x_2\sin(2\mu y) + x_3\sin(3\mu y)]$$

$$+\sin(2kx)[y_1\sin(\mu y) + y_2\sin(2\mu y) + y_3\sin(3\mu y)]$$

$$+\sin(3kx)[z_1\sin(\mu y) + z_2\sin(2\mu y) + z_3\sin(3\mu y)] \qquad (A1)$$

The nine equations governing the model are:

$$\frac{dx_1}{dt} = c_1x_2y_1 + c_2x_3y_2 + c_3y_2z_1 + c_4y_3z_2$$

$$+c_5x_2y_3 + c_6y_1z_2 + d_1h_1 + e_1x_1 \qquad (A.2)$$

$$\frac{dx_2}{dt} = c_7x_1y_1 + c_8y_1z_1 + c_9y_1z_3 + c_{10}y_3z_1$$

$$+c_{11}x_3y_1 + c_{12}x_1y_3 + d_2h_2 + e_2x_2 \qquad (A.3)$$

$$\frac{dx_3}{dt} = c_{13}x_1y_2 + c_{14}x_2y_1 + c_{15}y_1z_2$$

$$+c_{16}y_2z_1 + d_3h_3 + e_3x_3 \tag{A.4}$$

$$\frac{dy_1}{dt} = c_{17}x_1x_2 + c_{18}x_2x_3 + c_{19}x_3z_2 + c_{20}x_2z_3$$

$$+c_{21}x_1z_2 + c_{22}x_2z_1 + d_4h_4 + e_4y_1 \tag{A.5}$$

$$\frac{dy_2}{dt} = c_{23}x_3x_1 + c_{24}x_1z_1 + c_{25}x_3z_1$$

$$+d_5h_5 + e_5y_2 \tag{A.6}$$

$$\frac{dy_3}{dt} = c_{26}x_1x_2 + c_{27}x_1z_2 + c_{28}x_2z_1$$

$$+d_6h_6 + e_6y_3 \tag{A.7}$$

$$\frac{dz_1}{dt} = c_{29}x_2y_1 + c_{30}x_1y_2 + c_{31}x_3y_2 + c_{32}x_2y_3$$

$$+d_7h_7 + e_7z_1 \tag{A.8}$$

$$\frac{dz_2}{dt} = c_{33}x_1y_1 + c_{34}x_1y_3 + c_{35}x_3y_1$$

$$+d_8h_8 + e_8z_2 \tag{A.9}$$

$$\frac{dz_3}{dt} = c_{36}x_2y_1 + d_9h_9 + e_9z_3 \tag{A.10}$$

APPENDIX II

The coefficients entering the model equations will be listed in this appendix. The following notations have been introduced:

$$r = \frac{L}{W};\ k = \frac{2\pi}{L};\ q^2 = \frac{q_d^2}{k^2};$$

where L is the length of the channel and W is the width.

In addition, the following notations have been defined:

$$n_1 = 1 + r^2 + q^2;\ n_2 = 1 + 4r^2 + q^2;\ n_3 = 1 + 9r^2 + q^2$$

$$n_4 = 4 + r^2 + q^2;\ n_5 = 4 + 4r^2 + q_2;\ n_6 = 4 + 9r^2 + q^2$$

$$n_7 = 9 + r^2 + q^2;\ n_8 = 9 + 4r^2 + q_2;\ n_9 = 9 + 9r^2 + q^2$$

Using the above notations we may write the formulas for the c-coefficients in the following way:

$$c_1 = \frac{9r(1-r^2)}{4n_1};\ c_2 = \frac{r(3-5r^2)}{n_1};\ c_3 = \frac{r(5-3r^2)}{n_1}$$

$$c_4 = \frac{25r(1-r^2)}{4n_1};\ c_5 = \frac{r(3+5r^2)}{4n_1};\ c_6 = \frac{r(5+3r^2)}{4n_1}$$

$$c_7 = -\frac{9r}{4n_2};\ c_8 = -\frac{25r}{4n_2};\ c_9 = \frac{3r(5+8r^2)}{4n_2}$$

$$c_{10} = \frac{7r(5-8r^2)}{4n_2};\ c_{11} = \frac{5r(3-8r^2)}{4n_2};\ c_{12} = \frac{r(3+8r^2)}{4n_2}$$

$$c_{13} = -\frac{3r(1+r^2)}{n_3};\ c_{14} = -\frac{15r(1-r^2)}{4n_3};\ c_{15} = -\frac{7r(5+3r^2)}{4n_3}$$

$$c_{16} = -\frac{2r(5-3r^2)}{n_3};\ c_{17} = \frac{9r^3}{4n_4};\ c_{18} = \frac{25r^3}{4n_4}$$

$$c_{19} = \frac{7r(8-5r^2)}{4n_4};\ c_{20} = -\frac{3r(8+5r^2)}{4n_4};\ c_{21} = -\frac{r(8+3r^2)}{4n_4}$$

$$c_{22} = \frac{5r(8-3r^2)}{4n_4};\ c_{23} = \frac{8r^3}{n_5};\ c_{24} = -\frac{8r}{n_5}$$

$$c_{25} = \frac{16r(1-r^2)}{n_5};\ c_{26} = -\frac{3r^2}{4n_6};\ c_{27} = -\frac{5r(8+3r^2)}{4n_6}$$

$$c_{28} = -\frac{7r(8-3r^2)}{4n_6};\ c_{29} = -\frac{15r(1-r^2)}{4n_7};\ c_{30} = \frac{3r(1+r^2)}{d_7}$$

$$c_{31} = -\frac{2r(3-5r^2)}{n_7};\ c_{32} = \frac{7r(3+5r^2)}{4n_7};\ c_{33} = \frac{3r}{4n_8}$$

$$c_{34} = \frac{5r(3+8r^2}{4n_8};\ c_{35} = -\frac{7r(3-8r^2)}{4n_8};\ c_{36} = \frac{9r(1-r^2)}{4n_9}$$

The d-coefficients are listed as follows:

$$d_1 = \frac{\Gamma}{n_1};\ d_2 = \frac{\Gamma}{n_2};\ d_3 = \frac{\Gamma}{n_3}$$

$$d_4 = \frac{\Gamma}{n_4};\ d_5 = \frac{\Gamma}{n_5};\ d_6 = \frac{\Gamma}{n_6}$$

$$d_7 = \frac{\Gamma}{n_7};\ d_8 = \frac{\Gamma}{n_8};\ d_9 = \frac{\Gamma}{n_9}$$

Finally, the e-coefficients are as follows:

$$e_1 = -\frac{1+r^2}{n_1};\ e_2 = -\frac{1+4r^2}{n_2};\ -\frac{1+9r^2}{n_3}$$

$$e_4 = -\frac{4+r^2}{n_4};\ e_5 = -\frac{4(1+4r^2)}{n_5};\ e_6 = -\frac{4+9r^2}{n_6}$$

$$e_7 = -\frac{9+r^2}{n_7};\ e_8 = -\frac{9+4r^2}{n_8};\ e_9 = -\frac{9(1+r^2)}{n_9}$$

REFERENCES

Plaut, G. and R. Vautard, 1994. Spells of low-frequency oscillations and weather regimes in the Norther Hemisphere, *Jour. of Atmos. Sci.*, **51**, 210-236.

Wiin Christensen, C. and A. Wiin-Nielsen, 1996. Blocking as a wave-wave interaction, *Tellus*, **48A**, 254-271.

Wiin-Nielsen, A., 1991. The birth of numerical weather prediction, *Tellus*, **43AB**, 36-52 (see appendix).

Wiin-Nielsen, A., 1996. A note on longer term oscillations in the atmosphere, *Atmósfera*, **9**, pp. 222-240.